Effect of packing height and location of porous media on heat transfer in a cubical cavity Are extended Darcy simulations sufficient?

Chakkingal, Manu; Schiavo, Sabino; Ataei-Dadavi, Iman; Tummers, Mark J.; Kleijn, Chris R.; Kenjereš, Saša

DOI
10.1016/j.ijheatfluidflow.2020.108617

Publication date
2020

Document Version
Final published version

Published in
International Journal of Heat and Fluid Flow

Citation (APA)
Chakkingal, M., Schiavo, S., Ataei-Dadavi, I., Tummers, M. J., Kleijn, C. R., & Kenjereš, S. (2020). Effect of packing height and location of porous media on heat transfer in a cubical cavity: Are extended Darcy simulations sufficient? *International Journal of Heat and Fluid Flow*, *84*, Article 108617. https://doi.org/10.1016/j.ijheatfluidflow.2020.108617

International Journal of Heat and Fluid Flow 84 (2020) 108617

Contents lists available at ScienceDirect

International Journal of Heat and Fluid Flow

journal homepage: www.elsevier.com/locate/ijhff

Effect of packing height and location of porous media on heat transfer in a cubical cavity: Are extended Darcy simulations sufficient?

Manu Chakkingal[*,1,a], Sabino Schiavo[1,a], Iman Ataei-Dadavi[a], Mark J. Tummers[b], Chris R. Kleijn[a], Saša Kenjereš[a]

[a] Transport Phenomena Section, Department of Chemical Engineering, Delft University Of Technology, Delft, The Netherlands
[b] Fluid Mechanics Section, Department of Process and Energy, Delft University Of Technology, Delft, The Netherlands

ARTICLE INFO

Keywords:
Natural convection
Porous media
Partially filled
Shifted porous layer
Pore-structure resolved
Polyhedral mesh
Darcy-Forchheimer assumption
OpenFOAM
ANSYS-FLUENT

ABSTRACT

We numerically investigate natural convection in a bottom-heated top-cooled cavity, fully and partially filled with adiabatic spheres (with diameter-to-cavity-size ratio $d/L = 0.2$) arranged in a Simple Cubic Packing (SCP) configuration. We study the influence of packing height and location of porous media. We carry out the simulations using water as the working fluid with Prandtl number, $Pr = 5.4$ at Rayleigh number $Ra = 1.16 \times 10^5$, 1.16×10^6 and 2.31×10^7. The applicability and suitability of Darcy-Forchheimer assumption to predict the global heat transfer is analysed by comparing it with the pore-structure resolved simulations. We found that the heat transfer in pore-structure resolved simulations is comparable to that in fluid-only cavities at high Rayleigh numbers, irrespective of the number of layers of packing and its location. Discrepancies in heat transfer between the Darcy-Forchheimer and the fully resolved simulations are observed when the porous medium is close to the isothermal wall and at high *Ra*, while it vanishes when the porous medium is away from the isothermal bottom wall.

1. Introduction

Natural convective heat transfer in porous media packed cavities is of great importance in various engineering and real-life applications. It is an important mechanism in refrigeration devices Laguerre et al. (2008a,b), distribution transformers Torriano et al. (2018), nuclear waste disposal Shams et al. (2014), air dehumidifiers Fazilati et al. (2016), catalytic reactors Li et al. (2013); Thiagalingam et al. (2015), etc. It can also be of crucial importance in heat exchangers Boomsma et al. (2003); Missirlis et al. (2007) under safety mode operation, when the forced flow is blocked. In most of the applications mentioned above the domain may be partially filled Zhu et al. (2018) with materials and the relative position of these materials may vary (like food kept at the bottom or top of a refrigerator), which demands an in-depth understanding of the heat transfer mechanism in a partially filled porous media and its relative position.

Several experimental and numerical studies on natural convection in porous media are available in literature Nield et al. (2006). Most of the studies are on the influence of Rayleigh number Katto and Masuoka (1967), Prandtl number Catton and Jonsson (1987); Kladias and Prasad (1989), conductivity Zhao et al. (2005); Ataei-Dadavi et al. (2019b) and size of porous media Seki et al. (1978); Keene and Goldstein (2015); Nithiarasu et al. (1998). Studies also report that the heat transfer in fully packed porous media filled cavities asymptotically approach the heat transfer in a fluid-only cavity at high Rayleigh numbers Keene and Goldstein (2015); Ataei-Dadavi et al. (2019a). All these studies concentrate on the effect of the above mentioned parameters on fully packed cavities. However, the studies on the effect of location of the porous medium and its height are limited. Studies on partially filled porous media made of metal foam report a positive influence of porous media on heat transfer enhancement Kathare et al. (2008). The enhancement reported is mostly due to the increased conductivity of the medium. Experimental studies also report a non-monotonic change in heat transfer with packing height Prasad et al. (1991); Prasad (1993). Visualization from the top of the cavity hints at the channeling effect to be the reason for the non-monotonic heat transfer variation.

A variety of different cases and conditions were tested using Darcy assumption and other more refined Darcy models Nield et al. (2006), with most of them being 2D simulations. Semi-analytical solution for 2-dimensional Fahs et al. (2014, 2015) and 3-dimensional

* Corresponding author.
E-mail address: M.Chakkingal@tudelft.nl (M. Chakkingal).
[1] contributed equally to this manuscript.

https://doi.org/10.1016/j.ijheatfluidflow.2020.108617
Received 4 November 2019; Received in revised form 6 March 2020; Accepted 20 April 2020

Nomenclature

α	Thermal diffusivity,($\lambda/\rho c_p$), m^2/s
β	Thermal expansion coefficient, K^{-1}
λ	Thermal conductivity, W/m.K
λ_{eff}	Effective thermal conductivity, W/m.K
ν	Kinematic viscosity of fluid, m^2/s
ϕ	Porosity
ρ	Density, kg/m^3

Other symbols and Abbreviations

Ra	Rayleigh Number based on fluid properties, $\frac{g\beta_f \Delta T L^3}{\nu\alpha}$
Nu	Nusselt number based on fluid properties
Pr	Prandtl Number
θ	Non-dimensional temperature, $\frac{T - T_c}{T_h - T_c}$
θ_m	Time- and plane- averaged temperature
T	Temperature, K
T_{ref}	Reference temperature, $\frac{T_h + T_c}{2}$, K
c_p	Specific heat capacity, J/kg.K
d	Diameter of sphere, m
d_p	Diameter of pore-space, m
δ_{th}	Thermal boundary layer thickness,$\frac{L}{2Nu}$, m
L	Height of cavity, m
K	Permeability
Da	Darcy number, K/L^2
V_T^{porous}	Total volume of porous layer, m^3
$V_T^{spheres}$	Volume occupied by spheres, m^3
$\mathbf{u}$	Pore-scale velocity, m/s
$\mathbf{u}^*$	non-dimensional pore-scale velocity, $\frac{\mathbf{u}}{U_0}$
U_0	characteristic velocity scale, $\frac{Ra^{3/7}\alpha}{L}$, m/s
t_0	characteristic time scale, $\frac{L}{U_0}$, s
X, Y, Z	represents the rectangular coordinate system
D-F	Darcy-Forchheimer simulation with continuum approach
P-R	Pore-structure Resolved simulation
$\mathbf{g}$	accel. due to gravity (acts along Z axis), m/s^2
p	Pressure, N/m^2

Subscripts

eff	Effective
f	Fluid
s	Solid

Shao et al. (2018) porous media are available for conditions at which Darcy assumption is valid. 3-dimensional numerical simulation of layered porous structure with Darcy assumption Guerrero-Martínez et al. (2017) discusses the influence of the thermal properties of the layer in heat transfer. However, at comparatively higher flow velocities, this linear relation is valid only at lower Reynolds number Nield et al. (2006). Extensive studies on porous-continuum representative volume (REV) based approach Vafai (1984); Nithiarasu et al. (1998) valid at higher flow velocities, with Darcy Basak et al. (2007); Das et al. (2017) and Darcy-Forchheimer Das et al. (2016) terms included are reported in literature. Heat transfer in partially filled cavities, obtained using REV approach with Darcy and extended Darcy assumptions show good agreement with experiments at low *Ra* Bagchi and Kulacki (2011); Poulikakos (1986). The simulations, however, deviate up to 15% from the experimental heat transfer measurements, when the *Ra* and *Da* are high, and also with the change in the location and height of the packing Su et al. (2015).

From our literature review, we find that the literature on the effect of pore-scale phenomena on heat transfer is mostly limited to fully packed cavities Karani and Huber (2017); Chakkingal et al. (2019) and almost no literature is available on the effect of location and height of packing Laguerre et al. (2008b). From our previous numerical Chakkingal et al. (2019, 2020b, 2020a) and experimental Ataei-Dadavi et al. (2019a, 2019b, 2020) studies on fully-packed porous media, we find a strong influence of pore-scale features on global and local heat transfer. Consequently, detailed pore-structure resolved simulations can give us a better understanding of the effect of height and location of the packing on heat transfer as well as the reason for deviation of REV approach based simulations from experiments. In our present work, we carry out 3D numerical simulations resolving the pore-structure and compare them to the Darcy-Forchheimer (D-F) simulations. We investigate the validity and applicability of the D-F assumption in partially filled cavities of different packing heights and locations, by comparing it with the pore-structure resolved simulations. We aim at providing an insight into the influence of local flow and thermal structures on the heat transfer in these cavities and explain the discrepancy in heat transfer between the pore-structure resolved and D-F simulations.

2. Mathematical formulations and numerical methods

2.1. Geometry and boundary conditions

We study natural convection in a cubical $L \times L \times L$ cavity filled with adiabatic spheres of diameter, $d = 0.2L$ at $Ra = 1.16 \times 10^5$, 1.16×10^6 and 2.3×10^7. We use water ($Pr = 5.4$) as the working fluid. The gravity, $\mathbf{g}$ acts along the negative Z-axis of the Cartesian coordinate system. From our previous experimental study on natural convection in fully-packed cavity Ataei-Dadavi et al. (2019a), we find that spherical beads of the dimensions mentioned above result in its influence on heat transfer at low *Ra*, while the effect reduces with an increase in *Ra*. The bottom and top walls of the cubical cavity are maintained at uniform temperatures T_h and T_c ($T_h > T_c$) respectively. All the other vertical walls are adiabatic. Effects of packing height and packing location are investigated carrying out fully resolved numerical simulations and comparing with Darcy-Forchheimer simulations.

- **Packing height:**The domain is stacked with different number of horizontal layers (Fig. 1 and Table 1) of sphere-packing from the bottom wall to the top, arranged in a Simple Cubic Packing (SCP) fashion
- **Packing location:**The domain is stacked with single layer (and 2 layers) of spheres at different positions with respect to the bottom wall (Table 1) in an SCP fashion

No-slip boundary condition is applied at all the walls for both fully resolved and D-F simulations, and also at the spherical surfaces in the fully resolved packed bed simulations. We ensure that $\beta\Delta T \ll 1$ in all our simulations such that the Boussinesq approximation Gray and Giorgini (1976) is valid.

2.2. Governing equations and numerical method

The governing equations used for the simulations are split into two:

- Fully resolved simulations of fluid-only (Rayleigh-Bénard convection) and packed bed cavities using open-source finite volume CFD solver Foam Extend 4.0 Weller et al. (1998)

Table 1
Packing name referred in the current work and the corresponding packing scheme.

Packing name	Packing Scheme
1 Layer	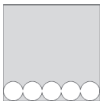
2 Layer	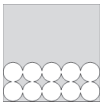
3 Layer	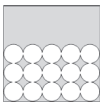
4 Layer	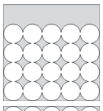
5 Layer	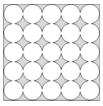
1L Middle	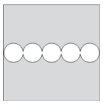
1L Quarter	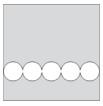
2L Quarter	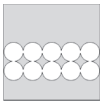

- Darcy-Forchheimer (D-F) simulations using commercial software, ANSYS Fluent (v17.2)

For the fully resolved simulations using the Boussinesq approximation, we numerically solve the transient Navier-Stokes and thermal energy transport equations for Newtonian fluids:

$$\nabla\cdot\,\mathbf{u} = 0 \tag{1}$$

$$\frac{\partial \mathbf{u}}{\partial t} + \mathbf{u}\cdot\nabla\mathbf{u} = -\frac{1}{\rho}\nabla p + \nu\nabla^2\mathbf{u} + \mathbf{g}\beta(T - T_{ref}) \tag{2}$$

$$\frac{\partial T}{\partial t} + \mathbf{u}\cdot\nabla T = \alpha\nabla^2 T \tag{3}$$

To perform fully resolved numerical simulations in our complex geometry, we use Foam Extend 4.0 (a fork of OpenFOAM). We use unstructured polyhedral grids Zenklusen et al. (2014, 2016) to carry out numerical simulations for the packed bed cavities and structured grids for the reference (fluid only) Rayleigh-Bénard convection simulations. The above set of equations, Eq. (1)-(3) are discretized and fully resolved numerical simulations are carried out using the standard solver **buoyantBoussinesqPisoFoam**. The solver is validated by comparing the heat transfer obtained at different *Ra* in fluid-only cavities to that reported in the literature Ataei-Dadavi et al. (2019a); Chu and Goldstein (1973); Valencia et al. (2005). A detailed solver validation is also reported in Chakkingal et al. (2020c). The heat transfer in cavity fully-filled with adiabatic spherical beads (discussed later) at the highest *Ra* reported, is compared to that obtained with glass beads, experimentally Ataei-Dadavi et al. (2019a). At $Ra = 2.31 \times 10^7$, for a cavity fully-filled with adiabatic spherical beads we obtain a Nusselt number, $Nu = 18.2$. From experiments it is observed that, at the same *Ra*, in a cavity filled with glass beads of the same size and packing Ataei-Dadavi et al. (2019a) we obtain a Nusselt number $Nu = 17.9$ (interpolated from data). The heat transfer obtained numerically with adiabatic beads is comparable to that obtained with glass beads (of lower conductivity) experimentally. This confirms the suitability of the current solver for the pore-structure resolved simulations of the packed bed.

Table 2
Numerical schemes for fully resolved simulations using OpenFOAM.

Settings	Numerical scheme
Time scheme	Backward (2^{nd} order)
Gradient scheme	Gauss linear, (2^{nd} order central)
Divergence scheme	Gauss limited linear
Laplacian scheme	Gauss linear corrected
Interpolation scheme	Linear
Pressure velocity coupling	PISO

We use the numerical schemes as listed in Table 2 to solve the convective and diffusive termsWeller et al. (1998) and to handle the pressure-velocity-coupling at each time step Issa (1986). The adaptive time-stepping is carried out by limiting the maximum cell Courant number to 0.33.

For the D-F simulations in ANSYS-Fluent, the effect of porous medium is modelled by including the pressure drop in a porous medium due to the viscous and inertial effects as a source term **S** in the momentum equation, Eq. 5 Nithiarasu et al. (1998).

$$\nabla\cdot\,\phi\mathbf{u} = 0 \tag{4}$$

$$\left(\frac{\partial \mathbf{u}}{\partial t} + \mathbf{u}\cdot\nabla\mathbf{u}\right) = -\frac{1}{\rho_f}\nabla p + \nu\nabla^2\mathbf{u} + \mathbf{g}\beta(T - T_{ref}) + \frac{1}{\rho_f}\mathbf{S} \tag{5}$$

$$(\rho c_p)^*\frac{\partial T}{\partial t} + (\rho c_p)_f\phi\mathbf{u}\cdot\nabla T = (\rho c_p)_f\alpha_{eff}\nabla^2 T \tag{6}$$

where,

- $(\rho c_p)^* = \phi(\rho c_p)_f + (1-\phi)(\rho c_p)_s$
- α_{eff} is calculated using an effective thermal conductivity, $\lambda_{eff} = \phi\lambda_f + (1-\phi)\lambda_s$, where λ_f and λ_s are the thermal conductivity of the fluid and solid (equal to zero in current simulations) respectively.

The source term, **S** in Eq. (5) is implemented as:

$$\mathbf{S} = -\frac{\mu}{C_0}\phi\mathbf{u} - C_1\frac{1}{2}\rho_f\phi\mathbf{u}|\phi\mathbf{u}| \tag{7}$$

For a packed bed cavity C_0 and C_1 are calculated using Ergun's equation as:

$$C_0 = \frac{d^2}{150}\frac{\phi^3}{(1-\phi)^2} \tag{8}$$

$$C_1 = \frac{3.5}{d}\frac{1-\phi}{\phi^3} \tag{9}$$

where d and ϕ are the diameter of the spherical beads and local porosity, respectively. For each packing scheme the packed bed section is substituted by a Darcy equivalent, both in position/size and properties. The porosity, ϕ is calculated for the porous layer using the porous layer height, L_H ($L_H = 0.2L$, $0.4L$ etc. for 1 Layer packing, 2 Layer packing etc. respectively) and the diameter of the sphere d as:

$$\phi = \frac{V_T^{\text{porous}} - V_T^{\text{spheres}}}{V_T^{\text{porous}}} \tag{10}$$

where, V_T^{porous} and V_T^{spheres} is the total volume of the cavity of height L_H and volume occupied by the spherical beads, respectively. The Eq. (4)-(7) in ANSYS Fluent user manual (when re-arranged) are the same as

Table 3
Numerical schemes for D-F simulations using Fluent.

Settings	Numerical scheme
Time scheme	2^{nd} order Implicit
Gradient	Least square Cell based
Momentum	Bounded Central differencing
Energy	Bounded Central differencing
Pressure	Second order
Pressure velocity coupling	PISO

reported in Nithiarasu et al. (1998). The details of solver validation are reported in Appendix A. For the investigated d/L ratio and porosity, the permeability K is equal to 1.05×10^{-6} resulting in a Da varying between 2.62×10^{-3} and 1.05×10^{-4} for packing height varying from 1 Layer to 5 Layers.

The governing equations in ANSYS-Fluent are solved using the numerical schemes listed in Table 3.

The time step size determined using for D-F simulations also satisfy the condition of maximum cell Courant number ≤ 0.33.

2.3. Mesh requirement

The pore-structure resolved (P-R) simulations are carried out using polyhedral mesh (Fig. 2(b)), generated by converting a fine tetrahedral mesh (Fig. 2(a)). The function *polyDualMesh* available in OpenFOAM is used to carry out this conversion. The number of mesh cells is decreased using this approach. For example, it reduces a 30 million cell tetrahedral mesh to a polyhedral mesh with around 6 million cells. Initial estimates of the grid requirement close to the wall and the bulk of the cavity are made based on the correlations provided in Shishkina et al. (2010) for Rayleigh-Bénard convection. Using the estimate for the highest $Ra = 2.3 \times 10^7$ as a base, a grid independence study is carried out using three different polyhedral meshes with 0.5 million, 4 million and 6 million cells for the cavity packed with 1 layer of spherical beads. The time-averaged integral Nusselt number (deviation less than 4%) and time- and plane- averaged non-dimensional temperature, θ_m along the vertical direction (Fig. 3) are used to ensure that we get a grid-independent solution. Though the volume of the packed-cavity to be meshed decreases with an increase in the number of layers of spherical beads, we use $\sim$ 6 million polyhedral cells to account for the increase in curved surfaces in the domain.

For the fluid-only and Darcy-Forchheimer simulations, we use structured hexahedral grid cells, with a growth factor of 1.2 close to the horizontal isothermal walls. A grid independence study is carried out using 32^3, 64^3 and 128^3 and 167^3 hexahedral cells. The deviation of time- and wall- averaged integral Nusselt number between 128^3 and 167^3 cells is less than 0.5% for $Ra = 2.3 \times 10^7$. All the reported results are thus obtained with the 128^3 hexahedral cells.

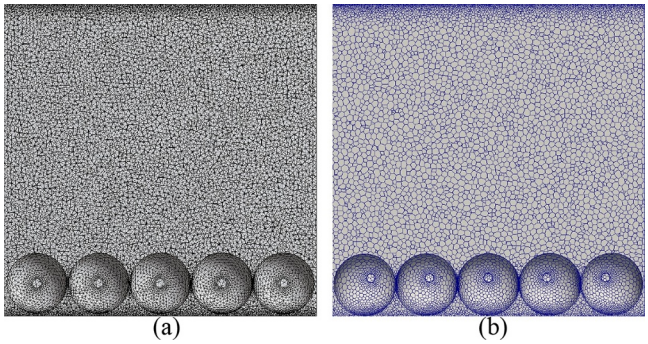

Fig. 2. Cubical cavity packed with 1 layer of adiabatic spherical beads meshed using (a) tetrahedral grids (b) polyhedral grids.

3. Results and Discussion

The influence of Rayleigh number, packing height and location of packing of spherical beads on the flow and heat transfer is discussed in this section. In the following sections, the ANSYS Fluent simulations with Darcy and Forchheimer terms are referred to as Darcy-Forchheimer (D-F) simulations. All the D-F simulations are carried with grid-size required to fully resolve the flow in the porous media free region. In the porous region we find the flow velocities to be very low such that the Reynolds number calculated with maximum flow velocity as the velocity scale and square root of permeability $\sqrt{K}$ as the length scale is ≈ 3 within the porous region. Thus laminar models are used for the simulations.

The pore-scale resolved simulations are compared to D-F simulations to better understand the suitability and applicability of D-F assumptions to simulate the flow and heat transfer in fully and partially packed porous domains. The results obtained with D-F simulations are also reported in terms of intrinsic velocity **u**. All the results reported below are expressed in non-dimensional form. The instantaneous temperature is non-dimensionalised using the temperature difference between the top and bottom wall as in $\theta = \frac{T - T_c}{T_h - T_c}$. The instantaneous intrinsic velocities, **u** are non-dimensionalized with the characteristic velocity scale $U_0 = \frac{{Ra_f}^{3/7}\alpha}{L}$ Castaing et al. (1989), such that the non-dimensional velocity vector **u*** equals

$$\mathbf{u}^* = \frac{\mathbf{u}}{U_0} \tag{11}$$

The time- and wall- averaged global heat transfer is expressed in terms of Nusselt number defined as:

$$Nu = -\frac{L}{\Delta T}\left(\frac{\partial T}{\partial z}\right)_{wall} \tag{12}$$

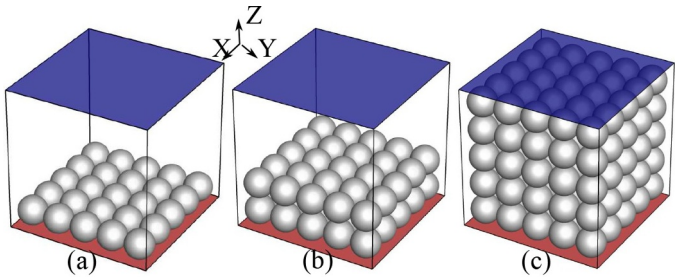

Fig. 1. Geometrical representation of fluid-filled cubical cavity heated from the bottom (red) and cooled from the top (blue) packed with (a) 1 layer (b) 2 layers (c) 5 layers of adiabatic spherical beads.

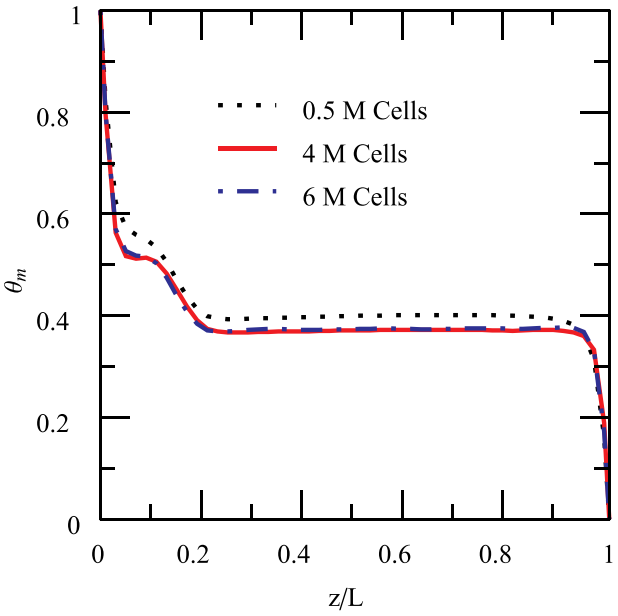

Fig. 3. Time- and plane- averaged mean temperature variation along Z direction in a cavity filled with 1 layer of spherical adiabatic beads for different mesh sizes at $Ra = 2.3 \times 10^7$.

3.1. Influence of Ra and packing height

We compare the heat transfer and flow features in P-R cavities with 1-5 layers of spherical beads stacked from the bottom to the top. The results from P-R simulations are compared with the D-F simulation results with the same local Darcy number Da and ϕ. We also compare the heat transfer obtained with P-R and D-F simulations to that in a fluid-only filled cavity.

In Fig. 4 we plot the time- and plane-averaged (averaged along XY plane) non-dimensional temperature of pore-structure resolved (P-R) simulations with 1 Layer to 5 Layer of spherical beads. The vertical lines indicate the packing height, for e.g. $z/L = 0.2$ and $z/L = 1$ represent the height of 1Layer packing and 5 Layer packing, respectively. At low $Ra = 1.16 \times 10^5$ (Fig. 4(a)), the temperature distribution becomes conduction-dominated with the increase in the number of layers of spherical beads i.e. from 1Layer to 5Layer packing. The "close to linear" temperature in fully-packed cavity (5 Layer) indicates the absence of convection in the cavity. The flow resistance imposed by the adiabatic spherical beads results in this behaviour.

In contrast to the above, at $Ra = 2.3 \times 10^7$ (Fig. 4(b)) the slope of time- and plane-averaged temperature close to the wall ($z/L = 0$ and $z/L = 1$) is comparable to that in a fluid-only filled cavity, indicating a convection dominated heat transfer. The presence of multi-layered adiabatic spherical beads results in an asymmetry in the temperature distribution, which vanishes in the cavity with 5 layers of packing.

From Fig. 5 we observe that the inclusion of spherical beads in the cavity, adversely affects the convective flow and thus the heat transfer is lower than in the fluid-only cavity, especially at low Ra. The non-dimensional heat transfer Nu in P-R cavities and in cavities with the D-F assumption are comparable at lower Rayleigh numbers ($Ra = 1.16 \times 10^5$, 1.16×10^6). At $Ra = 1.16 \times 10^5$ the heat transfer is much lower than in a fluid-only filled-cavity, and decreases with an increase in the number of layers of packing. At $Ra = 1.16 \times 10^6$, though the heat transfer is much lower than in fluid-only cavity, it is practically independent of the layers of packing (1 Layer-4 Layer). However, when the spherical beads are introduced close to the top cold wall (5 Layer), the heat transfer reduces further.

With the increase in Ra ($Ra = 2.3 \times 10^7$), the heat transfer in P-R cavities are slightly lower than (1 Layer-3 Layer, 5 Layer) or comparable (4 Layer) to that in fluid-only filled cavities, while the heat transfer obtained from simulations with D-F assumption is observed to be much lower than in the fluid-only cavities. The results from the P-R simulations are qualitatively similar to that obtained experimentally for partially filled Prasad et al. (1991) and fully-filled cavities Ataei-Dadavi et al. (2019a). Unlike the P-R simulations, the D-F simulations cannot capture this behaviour and thus significantly under-predict the heat transfer.

To understand the difference in heat transfer (Nu) between P-R and D-F simulations we analyse the instantaneous local Nusselt number, local non-dimensional temperature and the local non-dimensional velocity magnitude in cavities with 1 Layer and 5 Layer packing, at $Ra = 2.3 \times 10^7$.

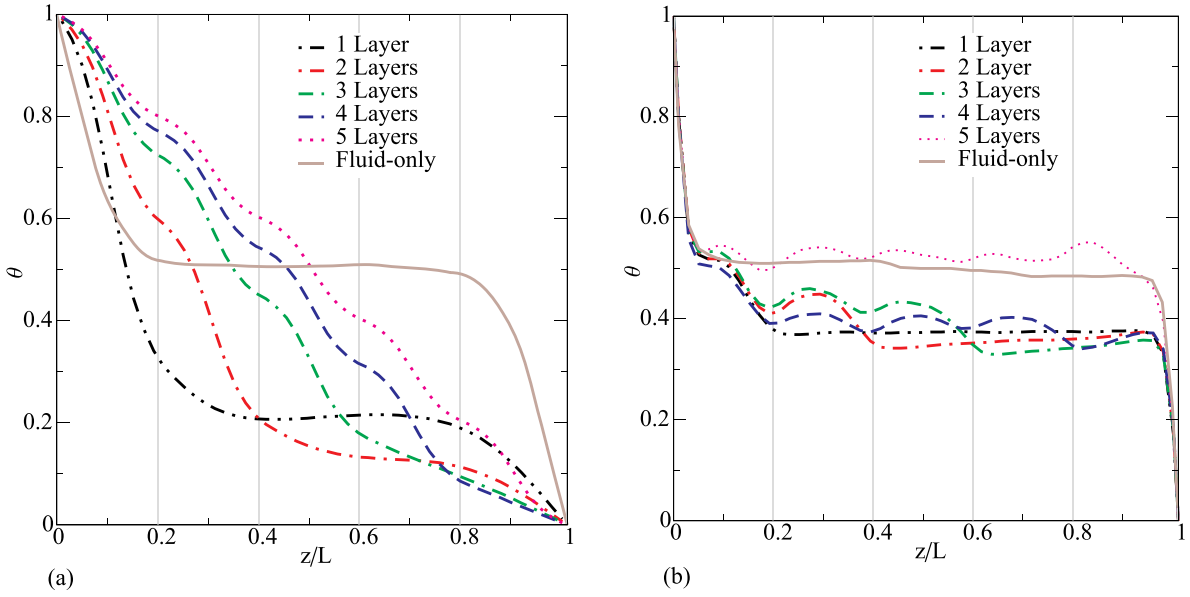

Fig. 4. Time- and plane- averaged non-dimensional temperature for cavities filled with different layers of spherical bead packing at (a) $Ra = 1.16 \times 10^5$, (b) $Ra = 2.3 \times 10^7$. Plane-averaging along planes with adiabatic spheres results in the wavy temperature distribution. The deviation in mean temperature from $\theta = 0.5$ for 5 layer packing indicates the need of time averaging for longer period.

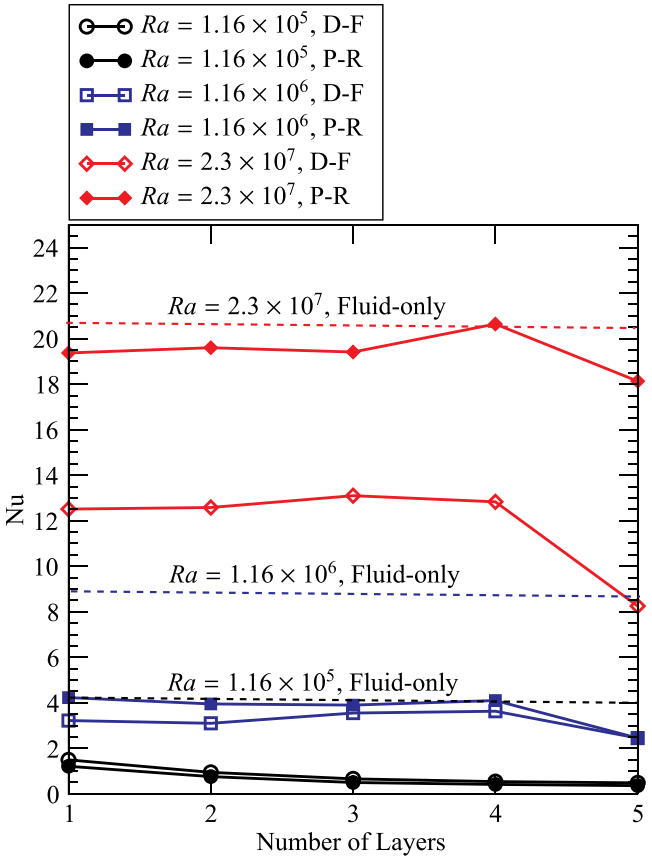

Fig. 5. Variation of time- and wall- averaged Nusselt number with number of layers of packing at different Rayleigh numbers. A comparison of pore-structure resolved (P-R) simulations is made with that from Darcy-Forchheimer (D-F) simulations and fluid-only filled cavity.

3.1.1. Darcy-Forchheimer simulations

In simulations with D-F assumption, the local Nusselt number (Fig. 6) at the bottom hot wall significantly decreases with the increase in the height of packing. In the D-F cavity with porous layer equivalent to the height of 1 Layer of spherical bead packing (Fig. 6(a)), the instantaneous heat transfer is high throughout the surface of the bottom wall. However, when the cavity is fully filled with porous media (Fig. 6(b)), the surface area with high local Nusselt number is smaller when compared to that in the cavity with 1 Layer of packing.

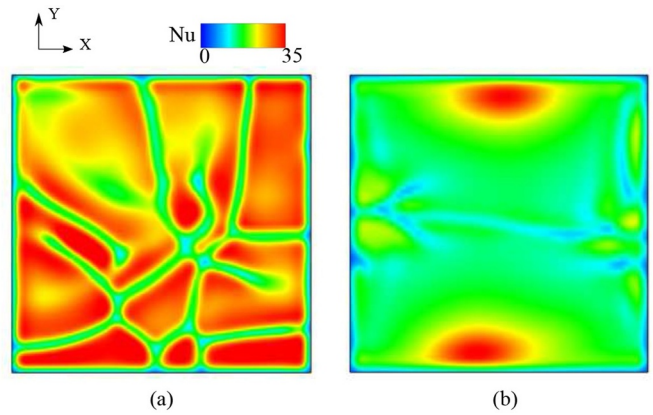

Fig. 6. Instantaneous Nusselt number distribution (top view) at the bottom wall, in a cavity with porous media filled to a height equivalent to (a)1 layer (b) 5 layers of spherical beads at $Ra = 2.3 \times 10^7$ obtained with Darcy-Forchheimer (D-F) simulations.

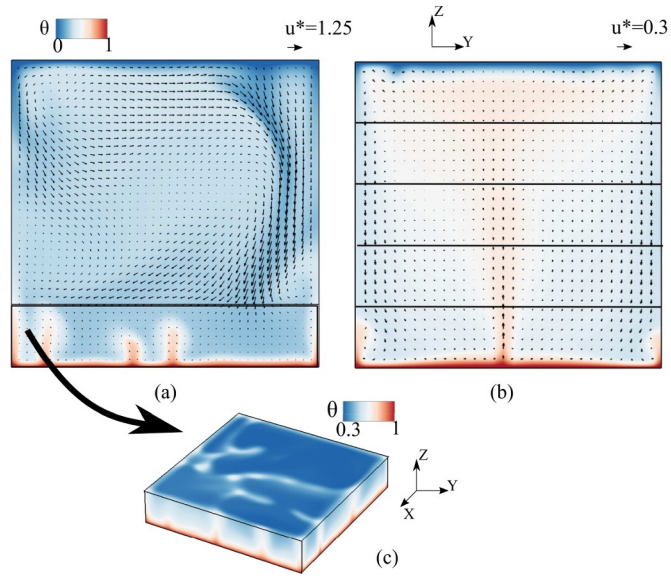

Fig. 7. Instantaneous non-dimensional temperature distribution and velocity vectors at $x/L = 0.43$, in a cavity with (a) 1 layer (layer height highlighted with a box) (b) 5 layers at $Ra = 2.3 \times 10^7$ simulated using Darcy-Forchheimer assumption. The velocity vectors are visualized by projecting them to a 32 × 32 grid along the vertical plane. The enlarged 3D view of the temperature distribution in the porous region of cavity with 1 Layer of packing is depicted in (c) with a different colour scale.

The reason for the reduction in heat transfer with the increase in porous layer height, becomes clear from the local non-dimensional instantaneous temperature (Fig. 7) and velocity magnitude (Fig. 8) along a plane ($X/L = 0.43$) in the configurations with 1 Layer and 5 Layers of packing. From Fig. 7(a) we see that the cold thermal plumes erupting from the top cold wall moves downward (as indicated by the velocity vectors) towards the bottom wall. From the velocity vectors we see that the flow in the porous region is lower when compared to the fluid-only region above the porous layer (Fig. 7(a)). The temperature at the interface of the fluid-only and porous region (Fig. 7(c)) is close to the cold fluid temperature. The fluid region above this interface thus behaves like a fluid only cavity.

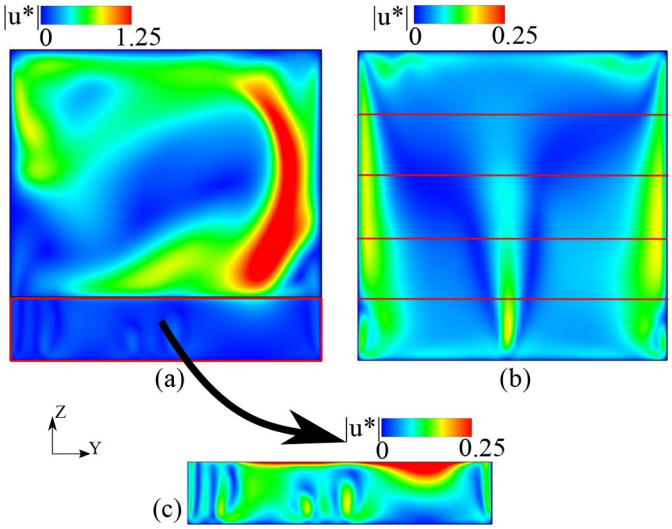

Fig. 8. Instantaneous non-dimensional velocity magnitude distribution at $x/L = 0.43$, in a cavity with (a) 1 layer (b) 5 layers at $Ra = 2.3 \times 10^7$ simulated using Darcy-Forchheimer assumption. The legend of (c) has a different scale from (a).

When the cavity is fully packed with porous media the asymmetry in temperature distribution (Fig. 7(b)) observed above, vanishes.The velocity vectors suggest the flow velocity to be much lower than that in the cavity with 1 Layer of packing (Fig. 7(a)). The contours of non-dimensional velocity magnitude confirm the reduction in flow velocity when the cavity is fully packed with porous media (Fig. 8(b)) when compared to the cavity with 1 Layer of packing (Fig. 8(a)). From Fig. 7 and Fig. 8 we find that the convective contribution to the heat transfer in the cavity decreases when the cavity is fully packed. The fluid-only region in the partially filled cavity dictates the total heat transfer thus resulting in a higher heat transfer (Fig. 6(a)) than in the fully-packed cavities (Fig. 6(b)).

3.1.2. *Pore-structure resolved simulations*

As observed in Fig. 5, the heat transfer obtained with pore-structure resolved simulations are comparable to that in fluid-only filled cavities and is higher than in D-F simulations, at high *Ra*. This is also evident from the local Nusselt number distribution of heat transfer at the bottom hot wall in P-R simulations, obtained in cavities with 1 Layer and 5 Layer of packing (Fig. 9). The local Nusselt number in P-R simulations (Fig. 9) are higher than in D-F simulations (Fig. 6). Unlike the Nusselt number distribution with D-F simulations, the heat transfer in P-R simulations are high in the regions close to the pore-space and are close to 0 at regions very close to the point of contact of the spherical beads with the bottom wall. To explain this behaviour, we look at the local flow and temperature in the plane $X/L = 0.43$, where the spherical beads and the pore-space are comparable in size. In Fig. 10 we compare configurations with 1 Layer (Fig. 10(a)) and 5 Layer (Fig. 10(b)) of spherical bead packing, at $Ra = 2.3 \times 10^7$. The instantaneous non-dimensional temperature contours also have the non-dimensional velocity vectors to give an indication of the direction and strength of the in-plane (ZY plane) flow. At the top right corner of the temperature contours we have the non-dimensional out-of plane velocity (u_x^*) contours.

From the temperature contours we observe that the thermal plumes erupting from the isothermal walls are thinner than the pore-space size (discussed later in next section), resulting in a flow-dominated heat transfer. This results in the heat transfer in spherical bead filled cavities to be comparable to that in a fluid-only filled cavity. Unlike the cavity with 1 Layer packing in which the flow is 3-dimensional with high value of out of plane velocity u_x^* (Fig. 10(a)), in the cavity with 5 Layer packing (Fig. 10(b)), we observe a channeled (2D planar) flow with negligible out of plane velocity. The slight increase in heat transfer observed with 4 Layer packing (Fig. 5) could be due to the dominance of the channeled flow in which the thin hot and cold plumes move through the pore-space and directly impinge on the cold and hot walls. However, a slight reduction in heat transfer occurs when the 5^{th} layer of spherical beads is placed close to the cold wall. Losing the area for the eruption of cold plumes in the cavity with 5 layers of packing results in this reduction, the effect of which is expected to diminish at higher *Ra* Ataei-Dadavi et al. (2019a); Chakkingal et al. (2019).

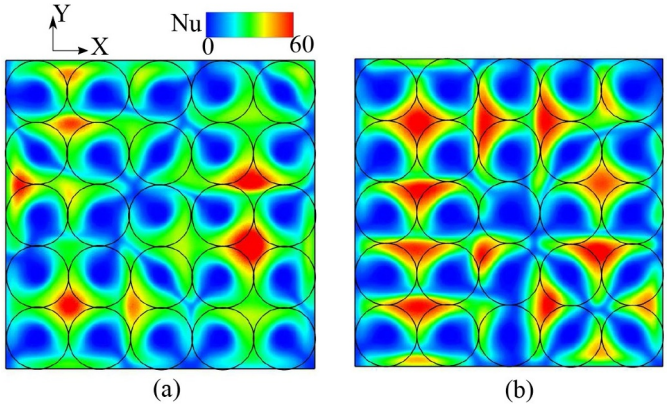

Fig. 9. Instantaneous Nusselt number distribution (top view) at the bottom wall, in a cavity with (a)1 layer (b) 5 layers of spherical beads at 2.3×10^7 obtained with pore-structure resolved (P-R) simulations.

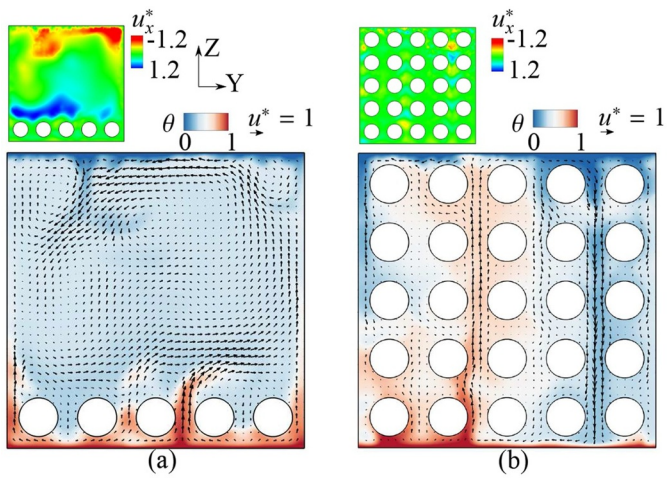

Fig. 10. Instantaneous non-dimensional temperature distribution and velocity vectors at $x/L = 0.43$, in a cavity with (a) 1 layer, (b) 5 layers of spherical beads at $Ra = 2.3 \times 10^7$. The smaller figure to the left of temperature contour depicts the non-dimensional out of plane velocity. The velocity vectors are visualized by projecting them to a 32 × 32 grid along the vertical plane.

To understand the local flow in P-R simulations, we look at the frequency spectra of thermal and kinetic energy at $Ra = 2.3 \times 10^7$ (of vertical velocity u_z) at the probe location ($y/L = 0.5$, $x/L = 0.6$, $z/L = 0.6$) in cavities with 1 Layer, 3 Layer and 5 Layer packing. The probe is far from the spherical beads in cavity with 1Layer packing, close to the beads in 3 Layer packing and within the pore-space in 5Layer packing. We also compare the spectra with that in a fluid-only cavity (same probe location) to understand the influence of spherical beads on local flow and thermal features.

The frequency spectra of thermal and kinetic energy at $Ra = 2.3 \times 10^7$ (of vertical velocity u_z) is turbulent in a fluid-only cavity following $E_T(f) \sim f^{-7/5}$ and $E_{u_z}(f) \sim f^{-11/5}$ comparable to that reported in Zhou and Xia (2001) and Shang and Xia (2001), respectively. From the P-R simulations of the spherical bead filled cavities, we observe that the temporal flow and temperature fluctuations (Fig. 11) dies out with the addition of layers of spherical beads. When we increase the number of the packing layers, the flow is still turbulent and thus the energy spectra follow the turbulent scaling for 1 Layer and 3 Layer packing, while the flow becomes oscillatory in the cavity with 5 Layer packing.

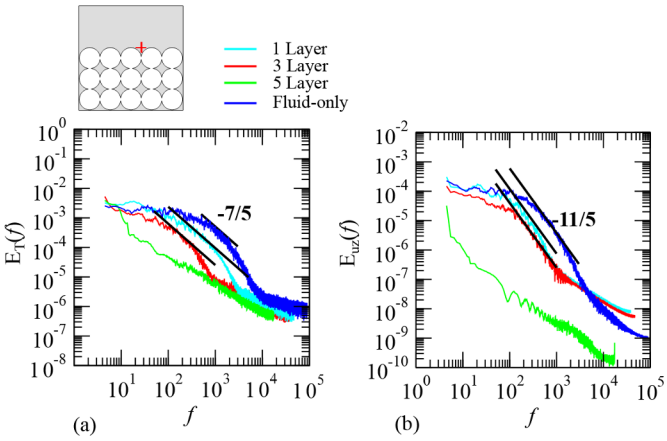

Fig. 11. Power-laws for the frequency (a) thermal energy spectra and (b) kinetic energy spectra of the vertical velocity u_z at $Ra = 2.3 \times 10^7$, $y/L = 0.5$, $x/L = 0.6$, $z/L = 0.6$.

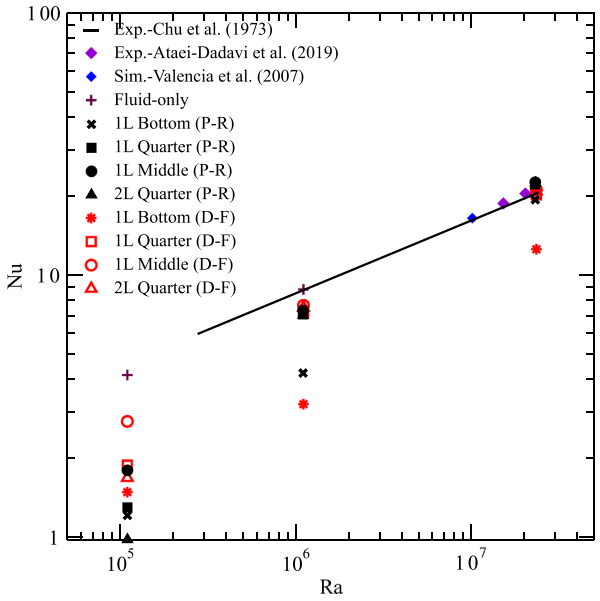

Fig. 12. Variation of *Nu* with *Ra* in pore-structure resolved (P-R) and Darcy-Forchheimer (D-F) simulations for different packing arrangement. The results are compared with heat transfer in fluid-only cavities reported in literature Ataei-Dadavi et al. (2019a); Chu and Goldstein (1973); Valencia et al. (2005). For naming convection of packing arrangement refer to Table 1.

This indicates that the flow becomes less turbulent as the relative distance of the probe with the spherical beads decreases, because of the increased resistance imposed by the spheres.

3.2. Influence of shift of packing

In contrast to the cavities with spherical beads touching the hot wall (Fig. 5), the suppression in heat transfer is comparatively lower when the spherical beads are shifted away from the hot wall (Fig. 12), both in P-R and D-F simulations.

3.2.1. Pore-structure resolved simulations

With P-R simulations, at $Ra = 1.16 \times 10^5$, for both 1 Layer and 2 Layer cases (Fig. 12), when the packing is away from the wall i.e for 1L/2L Quarter/Middle (P-R), the suppression in heat transfer varies significantly from that in cavities with the spherical beads touching the wall 1L/2L Bottom (P-R), for e.g. $Nu_{1\,\text{Layer Middle}} > Nu_{1\,\text{Layer Quarter}} > Nu_{1\,\text{Layer Bottom}}$. At higher *Ra* ($Ra = 1.6 \times 10^6$, 2.3×10^7), the heat transfer in porous media filled cavities with the packing away from the isothermal walls becomes comparable to or even slightly higher than that in fluid-only filled cavities, unlike the cavities in which the spherical beads touch the hot wall (1L Bottom (P-R)). To understand this difference in heat transfer behaviour, we look at the thermal plume (boundary layer) thickness defined as:

$$\delta_{th} = \frac{L}{2Nu}. \tag{13}$$

When the thermal plume size δ_{th} is scaled with the diameter of the pore-space d_p (Fig. 13), we observe that the thermal plumes are thicker than the pore-space ($\delta_{th}/d_p > 1$) at low *Ra* ($Ra = 1.16 \times 10^5$). While with the increase in *Ra*, thermal plumes become comparable to pore-size ($Ra = 1.16 \times 10^6$) and even gets smaller than the pore-size ($Ra = 2.31 \times 10^7$). At the lowest *Ra* ($Ra = 1.16 \times 10^5$), as the thermal plumes are thicker than the pore-space, the inclusion of the spherical beads leads to a considerable suppression in heat transfer as the thermal plumes cannot meander through the pore-space. The inclusion of spherical beads thus increases the resistance offered to the thermal plumes and even makes them thicker (Fig. 13).

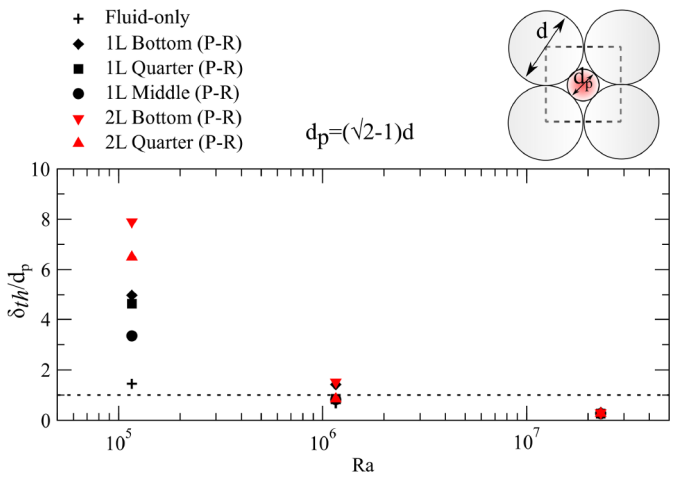

Fig. 13. Ratio of boundary layer thickness to pore-size at different *Ra*, for pore-scale resolved simulations. The boundary layer thickness of fluid-only cavity is also scaled with pore-size of the porous media filled-cavity for reference.

A comparison of the cavities with 1 Layer of packing (Fig. 12) shows that the suppression in heat transfer is minimum when the porous layer is at the center of the cavity (1L Middle (P-R)). This indicates that the influence of the packing on heat transfer decreases with the increase in its distance from the hot isothermal wall.

At $Ra = 1.16 \times 10^6$, as the thermal plume thickness of the fluid-only cavity is comparable to the pore-space (Fig. 13) and thus the reduction in heat transfer with the inclusion of spherical beads away from the isothermal walls is minimal (Fig. 12). This is also evident from the small change in the δ_{th}/d_p ratio in the cavities with spherical beads, when compared to the fluid-only filled cavity (Fig. 13). With the increase in *Ra* ($Ra = 2.31 \times 10^7$), the thermal plumes become much thinner than the pore-space (Fig. 13). The inclusion of layers of packing irrespective of their location, thus does not significantly obstruct the flow as the plumes meander through the pore-space. Thus at high *Ra*, the heat transfer in cavities with spherical beads are comparable to that in a fluid-only cavity (Fig. 12).

3.2.2. Darcy-Forchheimer simulations

At the lowest $Ra = 1.16 \times 10^5$, when the porous media touches the bottom hot wall, the heat transfer with with D-F and P-R simulations are comparable, for e.g. $Nu_{1\,\text{Layer Bottom}}$(D-F) $\approx$ $Nu_{1\,\text{Layer Bottom}}$(P-R) (Fig. 12).

However, the heat transfer obtained with the D-F simulations are lower than the P-R simulations at higher *Ra*, for e.g. at $Ra = 2.31 \times 10^7$, $Nu_{1\,\text{Layer Bottom}}$(D-F) $<$ $Nu_{1\,\text{Layer Bottom}}$(P-R). When the porous media is away from the isothermal hot wall, we observe a different behaviour.

- At $Ra = 1.16 \times 10^5$, *Nu* with D-F simulations are higher than with the P-R simulations (Fig. 12). This indicates that the flow within the pore-space of the spherical bead packing in P-R simulations is blocked as the thermal plumes are thicker than the pore-space (Fig. 13). While in the D-F simulations of the cavities with porous media not touching the isothermal walls, the convective flow is not fully choked as in P-R simulations, thus resulting in comparatively higher heat transfer (Fig. 12).
- At $Ra = 1.16 \times 10^6$ and $Ra = 2.31 \times 10^7$, the D-F and P-R simulations gives us comparable heat transfer, irrespective of the number of layers (Fig. 12).

We also observe that the resistance to the convective flow imposed by the porous media in D-F simulations is higher when it touches the isothermal wall when compared to the cavity with the porous media located away from it, thus resulting in lower heat transfer (Fig. 12), i.e. $Nu_{1\,\text{Layer Bottom}}$(D-F) $<$ $Nu_{1\,\text{Layer Quarter}}$(D-F).

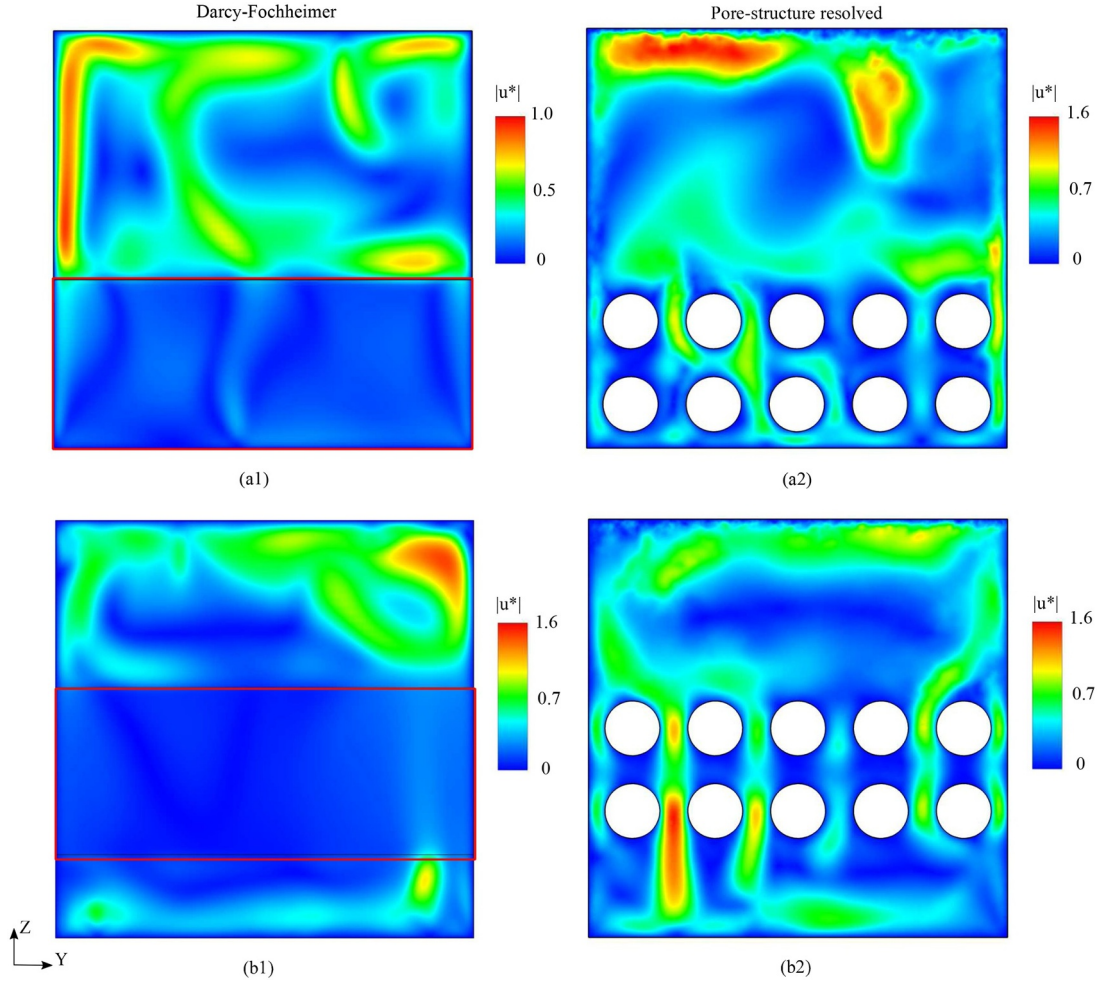

Fig. 14. Instantaneous non-dimensional velocity magnitude distribution at $x/L = 0.43$, in a cavity with 2 layers of spherical beads at $Ra = 2.3 \times 10^7$ in Darcy-Forchheimer (a1,b1) and pore-structure resolved (a2,b2) simulations. (a1,a2) has porous media from $z/L = 0$ to 0.4 and (b1, b2) has porous media from $z/L = 0.2$ to 0.6.

To understand the difference in the behaviour of the D-F simulations when the porous media touches the wall and when it is away from the wall, we look at the instantaneous non-dimensional velocity magnitude and temperature distribution along the plane, $X/L = 0.43$ in cavities with 2 Layer of porous media packing touching the isothermal wall (Fig. 14(a1), Fig. 15(a1)) and away from it (Fig. 14(b1), Fig. 15(b1)). We also compare it with the P-R simulations of the respective cavities (Fig. 14(a2,b2), Fig. 15(a2,b2)).

Since the thermal boundary layer is thinner than the pore-space at $Ra = 2.31 \times 10^7$ (Fig. 13), the pore-space flow velocity in the P-R simulation of the cavity with 2 Layer packing touching the bottom wall (Fig. 14(a2)), is less influenced by the spherical beads, resulting in hot thermal plumes at high velocity meandering through the pore-space (Fig. 15(a2)). In the cavities with porous media touching the isothermal hot wall, the flow velocity in the porous region obtained with D-F simulation (Fig. 14(a1)) is much lower than with the P-R simulation (Fig. 14(a2)). We also observe that in the simulation with D-F assumption, hot thermal plumes of comparatively lower temperature (Fig. 15(a1)) erupt from the bottom hot wall. Unlike the D-F simulation, the temperature and flow velocity of the hot thermal plumes (erupting from the bottom wall) within the pore-space is higher in the P-R simulation (Fig. 15(a2)). The combined effect of the thermal plume temperature and flow velocity results in lower convective heat transfer in the simulation with D-F assumption (Fig. 5).

However, in the D-F simulation with porous-media defined away from the wall (Fig. 14(b1)), the flow velocity close to the isothermal walls is less influenced by the porous media and is comparable to that in the P-R simulation (Fig. 14(b2)). Thus, comparable flow velocity close to the isothermal walls results in comparable heat transfer with D-F (2L Quarter (D-F)) and P-R (2L Quarter (P-R)) simulations (Fig. 12).

4. Summary and Conclusion

A detailed study on the validity and applicability of Darcy-Forchheimer assumption to simulate convective heat transfer in flow dominated porous media filled-cavity is reported. The Darcy-Forchheimer simulations of cavities with porous media touching the isothermal walls and away from them are compared with the pore-structure resolved simulations at different *Ra*. Major findings of this work can be summarized as:

(i) In cavities with porous media touching the isothermal wall, the heat transfer in simulations with Darcy-Forchheimer assumption is comparable to that in pore-structure resolved simulations at low *Ra*. With an increase in *Ra* the Darcy-Forchheimer simulations under-predict the heat transfer. At high *Ra*, the temperature and velocity of the thermal plumes impinging the hot wall are higher in the pore-structure resolved simulations resulting in heat transfer comparable to fluid-only cavities.
(ii) In cavities with porous media not touching the isothermal wall, Darcy-Forchheimer simulations and pore-structure resolved simulations report comparable heat transfer irrespective of the number

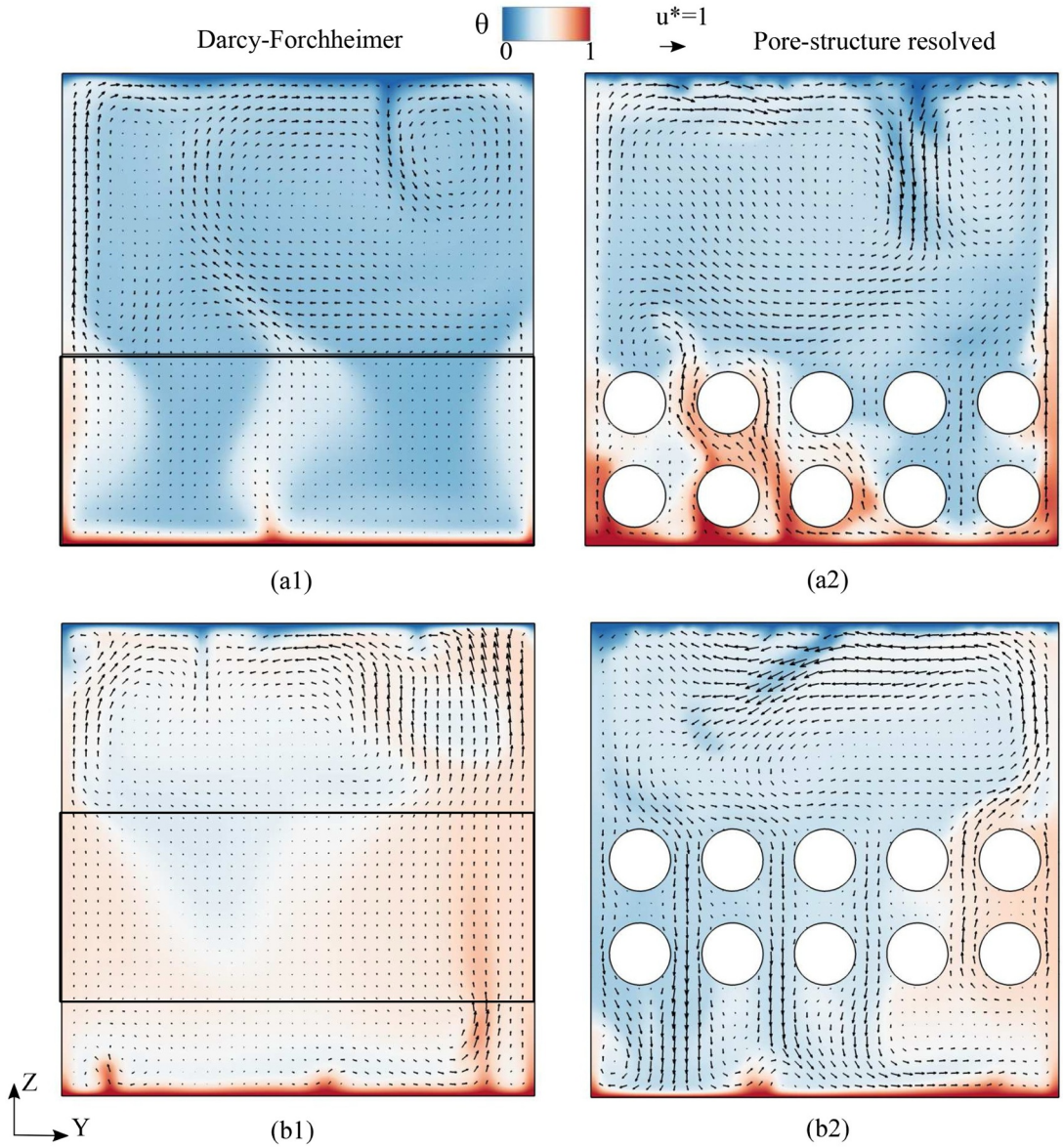

Fig. 15. Instantaneous non-dimensional temperature distribution and velocity vectors at $x/L = 0.43$, in a cavity with 2 layers of spherical beads at $Ra = 2.3 \times 10^7$ in Darcy-Forchheimer (a1,b1) and pore-scale resolved (a2,b2) simulations. (a1,a2) has porous media from $z/L = 0$ to 0.4 and (b1, b2) has porous media from $z/L = 0.2$ to 0.6.

of layers of packing and its location, for $Ra \geq 1.16 \times 10^6$. However, at low $Ra = 1.16 \times 10^5$ D-F simulations over-predict the heat transfer. This shows that the laminar model for porous-media simulations predicts heat transfer comparable to the pore-structure resolved simulations, when the non-porous regions are fully resolved.

(iii) Heat transfer in a porous medium filled-cavity decreases when the porous medium is close to the isothermal walls. A slight enhancement in heat transfer with porous media over the fluid-only cavity occurs when the channeling effect dominates over the effect due to the reduction in the area available for plume impingement when the packings are away from the isothermal walls.

(iv) From pore-structure resolved simulations, we observe that when the thermal boundary layer thickness (thermal plume size) is larger than the pore-space (of a pore-structure resolved cavity), the location and the number of layers of packing influence the heat transfer ($Ra = 1.16 \times 10^5$) for all packing configurations. However, it is practically independent of the porous packing when the boundary layer thickness is considerably smaller than the pore-size and when the porous media does not touch the wall (($Ra = 2.31 \times 10^7$). When the porous media touches the isothermal wall, the heat transfer is however reduced by the adiabatic spherical beads close to the wall. The reduction in heat transfer compared to fluid-only cavity is due to the comparatively lower flow velocity close to the wall.

Declaration of Competing Interest

The authors declare that they have no known competing financial interests or personal relationships that could have appeared to influence the work reported in this paper.

The authors declare the following financial interests/personal relationships which may be considered as potential competing interests:

CRediT authorship contribution statement

Manu Chakkingal: Conceptualization, Data curation, Formal analysis, Investigation, Methodology, Supervision, Validation,

Visualization, Writing - original draft. **Sabino Schiavo:** Data curation, Formal analysis, Investigation, Methodology, Validation, Visualization, Writing - original draft. **Iman Ataei-Dadavi:** Investigation, Visualization, Writing - review & editing. **Mark J. Tummers:** Project administration, Funding acquisition, Writing - review & editing. **Chris R. Kleijn:** Project administration, Resources, Software, Funding acquisition, Supervision, Writing - review & editing. **Saša Kenjereš:** Project administration, Resources, Visualization, Funding acquisition, Supervision, Writing - review & editing.

Acknowledgments

This research was carried out under project number S41.5.14526a in the framework of the Partnership Program of the Materials innovation institute M2i (www.m2i.nl) and the Technology Foundation TTW (www.stw.nl), which is part of the Netherlands Organization for Scientific Research (www.nwo.nl). We would like to thank our industrial partner TATA Steel, The Netherlands, for continuous financial support and SURFsara for the support in using the Cartesius Computing Cluster (NWO File No.17178).

Appendix A. Validation of Darcy-Forchheimer solver

To validate the Darcy-Forchheimer solver in ANSYS Fluent[2], we carry out 2D steady-state simulation of a differentially heated $L \times L$ cavity filled with porous media for fluid with $Pr = 1$ at $Da = 10^{-6}$, $Ra = 10^{8}$, $\phi = 0.8$ and $Da = 10^{-2}$, $Ra = 10^{4}$, $\phi = 0.6$, and carry out with the results reported in Das et al. (2016). The simulations are carried out in a 80 × 80 hexahedral grids of equal size. The isotherm (Fig. A.16) obtained with different Da and Ra are comparable to that reported in Das et al. (2016). A plot of the temperature along the horizontal line at the mid-height of the cavity (Fig. A.17) shows us that the results obtained with ANSYS Fluent are comparable to that in literature.

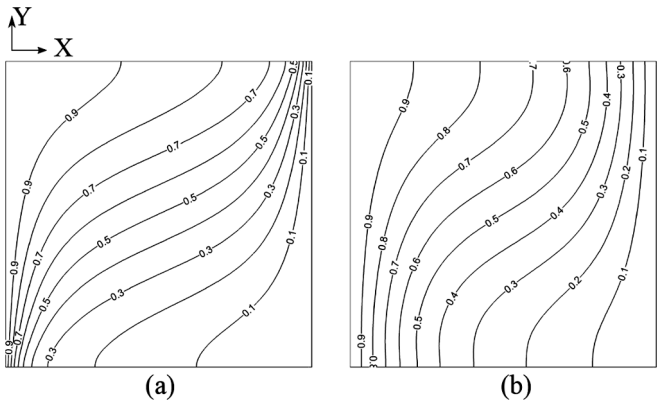

Fig. A1. Isotherms (θ) for (a) $Da = 10^{-6}$, $Ra = 10^{8}$, $\phi = 0.8$ (b) $Da = 10^{-2}$, $Ra = 10^{4}$, $\phi = 0.6$ using Darcy-Forchheimer assumption.

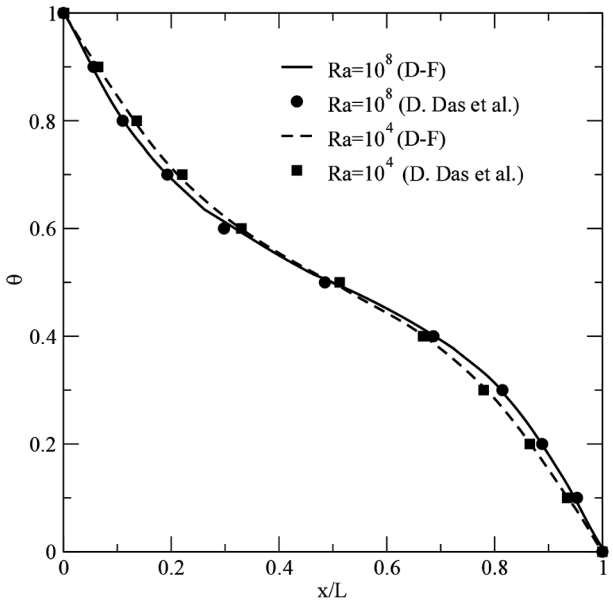

Fig. A2. Non-dimensional temperature (θ) along the line $y/L = 0.5$ for (a) $Da = 10^{-6}$, $Ra = 10^{8}$, $\phi = 0.8$ (b) $Da = 10^{-2}$, $Ra = 10^{4}$, $\phi = 0.6$ using Darcy-Forchheimer assumption. The current results are compared to that reported in Das et al. (2016).

[2] The validation is carried out using Second-order Upwind scheme for momentum and energy equations as central differencing schemes are not available for 2D simulations in Fluent.

References

Ataei-Dadavi, I., Chakkingal, M., Kenjeres, S., Kleijn, C.R., Tummers, M.J., 2020. Experiments on mixed convection in a vented differentially side-heated cavity filled with a coarse porous medium. International Journal of Heat and Mass Transfer 149, 119238. https://doi.org/10.1016/j.ijheatmasstransfer.2019.119238.

Ataei-Dadavi, I., Chakkingal, M., Kenjereš, S., Kleijn, C.R., Tummers, M.J., 2019. Flow and heat transfer measurements in natural convection in coarse-grained porous media. International Journal of Heat and Mass Transfer 130, 575–584. https://doi.org/10.1016/j.ijheatmasstransfer.2018.10.118.

Ataei-Dadavi, I., Rounaghi, N., Chakkingal, M., Kenjereš, S., Kleijn, C.R., Tummers, M.J., 2019. An experimental study of flow and heat transfer in a differentially side heated cavity filled with coarse porous media. International Journal of Heat and Mass Transfer 143, 118591. https://doi.org/10.1016/j.ijheatmasstransfer.2019.118591.

Bagchi, A., Kulacki, F.A., 2011. Natural convection in fluid–superposed porous layers heated locally from below. International Journal of Heat and Mass Transfer 54 (15-16), 3672–3682. https://doi.org/10.1016/j.ijheatmasstransfer.2011.01.034.

Basak, T., Roy, S., Takhar, H.S., 2007. Effects of nonuniformly heated wall(s) on a natural-convection flow in a square cavity filled with a porous medium. Numerical Heat Transfer, Part A: Applications 51 (10), 959–978. https://doi.org/10.1080/10407790601128600.

Boomsma, K., Poulikakos, D., Zwick, F., 2003. Metal foams as compact high performance heat exchangers. Mechanics of materials 35 (12), 1161–1176. https://doi.org/10.1016/j.mechmat.2003.02.001.

Castaing, B., Gunaratne, G., Heslot, F., Kadanoff, L., Libchaber, A., Thomae, S., Wu, X.-Z., Zaleski, S., Zanetti, G., 1989. Scaling of hard thermal turbulence in Rayleigh-Bénard convection. Journal of Fluid Mechanics 204 (-1), 1. https://doi.org/10.1017/s0022112089001643.

Catton, I., Jonsson, T., 1987. Prandtl Number Dependence of Natural Convection in Porous Media. Journal of Heat Transfer 109, 371–377. https://doi.org/10.1115/1.3248090.

Chakkingal, M., de Geus, J., Kenjereš, S., Ataei-Dadavi, I., Tummers, M.J., Kleijn, C.R., 2020. Assisting and opposing mixed convection with conjugate heat transfer in a differentially heated cavity filled with coarse-grained porous media. International Communications in Heat and Mass Transfer 111, 104457. https://doi.org/10.1016/j.icheatmasstransfer.2019.104457.

Chakkingal, M., Kenjereš, S., Ataei-Dadavi, I., Tummers, M.J., Kleijn, C.R., 2019. Numerical analysis of natural convection with conjugate heat transfer in coarse-grained porous media. International Journal of Heat and Fluid Flow 77, 48–60. https://doi.org/10.1016/j.ijheatfluidflow.2019.03.008.

Chakkingal, M., Kenjereš, S., Dadavi, I.A., Tummers, M.J., Kleijn, C.R., 2020. Numerical analysis of natural convection in a differentially heated packed bed with non-uniform wall temperature. International Journal of Heat and Mass Transfer 149, 119168. https://doi.org/10.1016/j.ijheatmasstransfer.2019.119168.

Chakkingal, M., Voigt, R., Kleijn, C.R., Kenjereš, S., 2020. Effect of double-diffusive convection with cross gradients on heat and mass transfer in a cubical enclosure with adiabatic cylindrical obstacles. International Journal of Heat and Fluid Flow (Accepted).

Chu, T.Y., Goldstein, R.J., 1973. Turbulent convection in a horizontal layer of water. Journal of Fluid Mechanics 60 (1), 141–159. https://doi.org/10.1017/s0022112073000091.

Das, D., Biswal, P., Roy, M., Basak, T., 2016. Role of the importance of 'forchheimer term' for visualization of natural convection in porous enclosures of various shapes. International Journal of Heat and Mass Transfer 97, 1044–1068. https://doi.org/10.1016/j.ijheatmasstransfer.2015.12.026.

Das, D., Roy, M., Basak, T., 2017. Studies on natural convection within enclosures of various (non-square) shapes – a review. International Journal of Heat and Mass Transfer 106, 356–406. https://doi.org/10.1016/j.ijheatmasstransfer.2016.08.034.

Fahs, M., Younes, A., Makradi, A., 2015. A reference benchmark solution for free convection in a square cavity filled with a heterogeneous porous medium. Numerical Heat Transfer, Part B: Fundamentals 67 (5), 437–462. https://doi.org/10.1080/10407790.2014.977183.

Fahs, M., Younes, A., Mara, T.A., 2014. A new benchmark semi-analytical solution for density-driven flow in porous media. Advances in Water Resources 70, 24–35. https://doi.org/10.1016/j.advwatres.2014.04.013.

Fazilati, M.A., Sedaghat, A., Alemrajabi, A.A., 2016. Natural induced flow due to concentration gradient in a liquid desiccant air dehumidifier. Applied Thermal Engineering 105, 105–117. https://doi.org/10.1016/j.applthermaleng.2016.05.135.

Gray, D.D., Giorgini, A., 1976. The validity of the Boussinesq approximation for liquids and gases. International Journal of Heat and Mass Transfer 19 (5), 545–551. https://doi.org/10.1016/0017-9310(76)90168-X.

Guerrero-Martínez, F.J., Younger, P.L., Karimi, N., Kyriakis, S., 2017. Three-dimensional numerical simulations of free convection in a layered porous enclosure. International Journal of Heat and Mass Transfer 106, 1005–1013. https://doi.org/10.1016/j.ijheatmasstransfer.2016.10.072.

Issa, R.I., 1986. Solution of the implicitly discretised fluid flow equations by operator-splitting. Journal of Computational Physics 62 (1), 40–65. https://doi.org/10.1016/0021-9991(86)90099-9.

Karani, H., Huber, C., 2017. Role of thermal disequilibrium on natural convection in porous media: insights from pore-scale study. Physical Review E 95 (3), 033123. https://doi.org/10.1103/PhysRevE.95.033123.

Kathare, V., Kulacki, F.A., Davidson, J.H., 2008. Buoyant convection in superposed metal foam and water layers. ASME 2008 Heat Transfer Summer Conference collocated with the Fluids Engineering, Energy Sustainability, and 3rd Energy Nanotechnology Conferences. American Society of Mechanical Engineers, pp. 217–223.

Katto, Y., Masuoka, T., 1967. Criterion for the onset of convective flow in a fluid in a porous medium. International Journal of Heat and Mass Transfer 10 (3), 297–309. https://doi.org/10.1016/0017-9310(67)90147-0.

Keene, D.J., Goldstein, R.J., 2015. Thermal convection in porous media at high Rayleigh numbers. Journal of Heat Transfer 137 (3), 034503. https://doi.org/10.1115/1.4029087.

Kladias, N., Prasad, V., 1989. Natural Convection in Horizontal Porous Layers: Effects of Darcy and Prandtl Numbers. Journal of Heat Transfer 111 (4), 926–935. https://doi.org/10.1115/1.3250807.

Laguerre, O., Amara, S.B., Alvarez, G., Flick, D., 2008. Transient heat transfer by free convection in a packed bed of spheres: Comparison between two modelling approaches and experimental results. Applied Thermal Engineering 28 (1), 14–24. https://doi.org/10.1016/j.applthermaleng.2007.03.014.

Laguerre, O., Amara, S.B., Charrier-Mojtabi, M.-C., Lartigue, B., Flick, D., 2008. Experimental study of air flow by natural convection in a closed cavity: Application in a domestic refrigerator. Journal of Food Engineering 85 (4), 547–560. https://doi.org/10.1016/j.jfoodeng.2007.08.023.

Li, X., Cai, J., Xin, F., Huai, X., Guo, J., 2013. Lattice boltzmann simulation of endothermal catalytic reaction in catalyst porous media. Applied Thermal Engineering 50 (1), 1194–1200. https://doi.org/10.1016/j.applthermaleng.2012.08.058.

Missirlis, D., Yakinthos, K., Storm, P., Goulas, A., 2007. Modeling pressure drop of inclined flow through a heat exchanger for aero-engine applications. International Journal of Heat and Fluid Flow 28 (3), 512–515. https://doi.org/10.1016/j.ijheatfluidflow.2006.06.005.

Nield, D.A., Bejan, A., et al., 2006. Convection in porous media. Vol. 3 Springer.

Nithiarasu, P., Seetharamu, K.N., Sundararajan, T., 1998. Effect of porosity on natural convective heat transfer in a fluid saturated porous medium. International Journal of Heat and Fluid Flow 19 (1), 56–58. https://doi.org/10.1016/s0142-727x(97)10008-x.

Poulikakos, D., 1986. Buoyancy-driven convection in a horizontal fluid layer extending over a porous substrate. The Physics of fluids 29 (12), 3949–3957. https://doi.org/10.1063/1.865734.

Prasad, V., 1993. Flow instabilities and heat transfer in fluid overlying horizontal porous layers. Experimental thermal and fluid science 6 (2), 135–146. https://doi.org/10.1016/0894-1777(93)90023-C.

Prasad, V., Brown, K., Tian, Q., 1991. Flow visualization and heat transfer experiments in fluid-superposed packed beds heated from below. Experimental Thermal and Fluid Science 4 (1), 12–24. https://doi.org/10.1016/0894-1777(91)90017-L.

Seki, N., Fukusako, S., Inaba, H., 1978. Heat transfer in a confined rectangular cavity packed with porous media. International Journal of Heat and Mass Transfer 21 (7), 985–989. https://doi.org/10.1016/0017-9310(78)90190-4.

Shams, A., Roelofs, F., Komen, E., Baglietto, E., 2014. Large eddy simulation of a randomly stacked nuclear pebble bed. Computers & Fluids 96, 302–321. https://doi.org/10.1016/j.compfluid.2014.03.025.

Shang, X.-D., Xia, K.-Q., 2001. Scaling of the velocity power spectra in turbulent thermal convection. Physical Review E 64 (6), 065301. https://doi.org/10.1103/PhysRevE.64.065301.

Shao, Q., Fahs, M., Hoteit, H., Carrera, J., Ackerer, P., Younes, A., 2018. A 3-d semi-analytical solution for density-driven flow in porous media. Water Resources Research 54 (12). https://doi.org/10.1029/2018wr023583.

Shishkina, O., Stevens, R.J., Grossmann, S., Lohse, D., 2010. Boundary layer structure in turbulent thermal convection and its consequences for the required numerical resolution. New Journal of Physics 12 (7), 075022. https://doi.org/10.1088/1367-2630/12/7/075022.

Su, Y., Wade, A., Davidson, J.H., 2015. Macroscopic correlation for natural convection in water saturated metal foam relative to the placement within an enclosure heated from below. International Journal of Heat and Mass Transfer 85, 890–896. https://doi.org/10.1016/j.ijheatmasstransfer.2015.02.022.

Thiagalingam, I., Dallet, M., Bennaceur, I., Cadalen, S., Sagaut, P., 2015. Exact non local expression for the wall heat transfer coefficient in tubular catalytic reactors. International Journal of Heat and Fluid Flow 54, 97–106. https://doi.org/10.1016/j.ijheatfluidflow.2015.03.007.

Torriano, F., Campelo, H., Quintela, M., Labbé, P., Picher, P., 2018. Numerical and experimental thermofluid investigation of different disc-type power transformer winding arrangements. International Journal of Heat and Fluid Flow 69, 62–72. https://doi.org/10.1016/j.ijheatfluidflow.2017.11.007.

Vafai, K., 1984. Convective flow and heat transfer in variable-porosity media. Journal of Fluid Mechanics 147 (-1), 233. https://doi.org/10.1017/s002211208400207x.

Valencia, L., Pallares, J., Cuesta, I., Grau, F.X., 2005. Rayleigh-bénard convection of water in a perfectly conducting cubical cavity: effects of temperature-dependent physical properties in laminar and turbulent regimes. Numerical Heat Transfer, Part A: Applications 47 (4), 333–352. https://doi.org/10.1080/10407780590889130.

Weller, H.G., Tabor, G., Jasak, H., Fureby, C., 1998. A tensorial approach to computational continuum mechanics using object-oriented techniques. Computers in Physics 12 (6), 620–631. https://doi.org/10.1063/1.168744.

Zenklusen, A., Kenjereš, S., von Rohr, P.R., 2014. Vortex shedding in a highly porous structure. Chemical Engineering Science 106, 253–263. https://doi.org/10.1016/j.ces.2013.11.022.

Zenklusen, A., Kenjereš, S., von Rohr, P.R., 2016. Mixing at high schmidt number in a complex porous structure. Chemical Engineering Science 150, 74–84. https://doi.org/10.1016/j.ces.2016.04.057.

Zhao, C.Y., Lu, T.J., Hodson, H.P., 2005. Natural convection in metal foams with open cells. International Journal of Heat and Mass Transfer 48 (12), 2452–2463. https://doi.org/10.1016/j.ijheatmasstransfer.2005.01.002.

Zhou, S.-Q., Xia, K.-Q., 2001. Scaling properties of the temperature field in convective turbulence. Physical review letters 87 (6), 064501. https://doi.org/10.1103/PhysRevLett.87.064501.

Zhu, Z.-Q., Huang, Y.-K., Hu, N., Zeng, Y., Fan, L.-W., 2018. Transient performance of a PCM-based heat sink with a partially filled metal foam: Effects of the filling height ratio. Applied Thermal Engineering 128, 966–972. https://doi.org/10.1016/j.applthermaleng.2017.09.047.